Joint International Topical Meeting on Mathematics & Computation and Supercomputing in Nuclear Applications (M&C + SNA 2007)
Monterey, California, April 15-19, 2007, on CD-ROM, American Nuclear Society, LaGrange Park, IL (2007)

A NEW ELECTRON ENERGY-LOSS STRAGGLING ALGORITHM IN MCNP

Lee T. Harding and Anil K. Prinja
University of New Mexico
Chemical and Nuclear Engineering Department
Albuquerque, NM 87131
lharding@unm.edu; prinja@unm.edu

H. Grady Hughes
Los Alamos National Laboratory
Group X-3, MS A143
Los Alamos, NM 87545
hgh@lanl.gov

ABSTRACT

A new algorithm for energy-loss straggling in MCNP is demonstrated. An approximate but accurate energy-loss moment-preserving differential cross section is used in conjunction with single event Monte Carlo simulation through each condensed history step to show that highly accurate energy spectra, leakage currents, and dose profiles can be obtained. This new approach provides a viable and even preferred alternative to the Landau straggling model currently employed in MCNP.

Key Words: Straggling, Condensed History, Moment-Preserving, MCNP

1. INTRODUCTION

In this paper, we describe and demonstrate an improved condensed history (CH) [1] electron energy-loss straggling model in MCNP. In most CH implementations [2–4], electron energy losses are sampled from the Landau distribution [1, 6] which is an approximate solution to the transport equation that ignores deflection. The model strives to accurately preserve the mean and mean-square energy loss moments of the analog cross section, i.e., the stopping power and straggling coefficient, and is accurate at high energies and for thin slabs, but the method is difficult to generalize when it is necessary to incorporate higher order moments. Here we propose a different method for accurately computing the straggling distribution, based on simulating the electron energy loss through each step by single event Monte Carlo in conjunction with a simplified energy-loss cross section. This new straggling model and algorithm has been implemented and tested in MCNP and shown to be potentially more accurate than the traditional method based on sampling the Landau distribution. In the ensuing we present the methodology as well as several demonstrative numerical results.

2. ELECTRON ENERGY-LOSS STRAGGLING

In the CH method, straggling distributions are ideally given by solutions to the following transport equation without deflection,

$$\frac{\partial\psi(s,E)}{\partial s} = \int_{Q_{min}}^{Q_{max}} \Sigma_{e^-}(E+Q,Q)\psi(s,E+Q)\,\mathrm{d}Q - \Sigma_{e^-}(E)\psi(s,E), \tag{1}$$

where $\psi(s,E)$ is the flux as a function of pathlength s and energy E, $\Sigma_{e^-}(E)$ is the total cross section, $\Sigma_{e^-}(E+Q,Q)$ is the differential cross section for energy loss Q in a collision which is often approximated by the Rutherford cross section but for electrons is more accurately given by the Møller formula [8]. The maximum energy transfer possible Q_{max} is given by the collision kinematics, accounting for the indistinguishability of incident and recoiling electrons [8]. The minimum energy Q_{min} is set equal to the mean ionization energy of the target atom so that our investigations are restricted to hard collisions only. The incorporation of mean and mean-square energy losses associated with soft (sub-ionization threshold) collisions is quite straightforward in our method and depends only on the availability of relevant models or data for these moments.

The Landau distribution [6] represents a solution to Eq.(1) subject to two important approximations. First, the mean free path of the electron is held constant throughout the step, amounting to fixing E at its initial value, and second, Q_{max} is allowed to become unbounded. Both approximations were introduced to facilitate analytic solution of Eq.(1) using a Laplace transform in the energy variable. The subsequent inverse transform, while not possible in closed form, was simplified enough to be numerically evaluated and stored for sampling. The first approximation requires the mean energy loss to be small compared to the incident electron energy, while the second is justified on the grounds that the differential cross section for large energy transfers varies as $\sim 1/Q^2$ so that relaxing the upper bound should not measurably affect the result. While the former approximation is reasonable for sufficiently thin layers or small step sizes, the second, however, results in the Landau distribution yielding an unbounded mean energy loss. This then necessitates the application of an artificial cut-off in the spectrum to ensure that the mean energy loss remains finite. We next describe our alternative approach which does not require the above approximations.

2.1. Moment Preserving Cross Sections

Key to our approach is the accurate and inexpensive solution of the straggling equation given by Eq.(1) over a step length. This is clearly not feasible when the true or analog differential cross section is employed but we have recently demonstrated that *modeled* differential cross sections can be constructed which are capable of yielding accurate straggling distributions over length scales comparable to step sizes used in CH implementations [5, 7, 9] provided, that is, they are constructed to preserve a sufficient number of energy-loss moments of the analog cross section defined by,

$$Q_n = \int_{Q_{min}}^{Q_{max}} \mathrm{d}Q\, Q^n \Sigma_{e^-}(E,Q), \quad n = 1, 2 \ldots. \tag{2}$$

No attempt is made to preserve the true mean free path but it has been demonstrated that if lower order moments of the true cross section, such as the mean and mean-square energy losses which capture the bulk of the dominating small energy transfers, are rigorously preserved while higher order moments, describing less frequent larger energy transfers, are reasonably accurately approximated, the resulting modeled cross section tends to be considerably smoother and the mean free path considerably longer [5, 7, 9]. This greatly

facilitates the numerical solution of Eq.(1) by any method and by Monte Carlo in particular, as we demonstrate below.

Clearly, there is no unique method for constructing moment-preserving approximations to the analog cross section, but we have identified two formulations that work extremely well. In one, we use a cross section representation that preserves a preset number of energy-loss moments through a superpostion of discrete energy losses. While a purely discrete cross section representation is ideal for sampling energy losses in Monte Carlo, discrete artifacts arise which have the potential to dominate the straggling distribution. To mitigate these artifacts, we supplement the discrete representation with a continuous-in-energy component in our second approach, to create a hybrid discrete-continuous cross section. Specifically, we use the exact Møller differential cross section to describe large energy transfer collisions and a discrete component to ensure lower moments are preserved. An interpolating parameter is introduced to connect the two components. The following sections describe, in detail, the purely discrete and hybrid energy-loss models.

2.1.1 Purely Discrete Energy-Loss Model

Using discrete distributions to represent cross sections is not new and was originally used to approximate elastic scattering[10]:

$$\Sigma^*_{el}(E,\mu_0) = \sum_{l=1}^{L} \frac{\gamma_l(E)}{2\pi}\delta[\mu_0 - \xi_l(E)], \tag{3}$$

where $\Sigma_{el}(E,\mu_0)$ is the approximate elastic scattering cross section for a particle with incident scattering cosine μ_0, and incident energy E. In Eq.(3), ξ_l are the discrete scattering cosines with their corresponding amplitudes γ_l, for $l = 1, 2 \ldots L$. The scattering angles and amplitudes are constrained to exactly yield the first $2L$ Legendre moments or momentum transfer moments of the analog differential elastic scattering cross section, the latter being given by

$$\Sigma_{n,el,mom}(E) = 2\pi \int_{-1}^{1} \mathrm{d}\mu_0 (1-\mu_0)^n \Sigma_{el}(E,\mu_0),\ n = 1, 2 \ldots. \tag{4}$$

Due to the similarities in the cross sections (i.e. steep cross sections for decreasing energies and steep cross sections for small angle scatters), it is possible to extend the idea of a discrete distribution to represent the continuous angular distribution to a discrete energy-loss distribution. With this we can represent the differential energy-loss cross section as a superposition of discrete energy-losses,

$$\Sigma^*_{e^-}(E,Q) = \sum_{l=1}^{L} \alpha_l \delta[Q - \overline{Q}_l]. \tag{5}$$

In Eq.(5), $\overline{Q}_l$ are the discrete energy losses with corresponding weights α_l, for $l = 1, 2 \ldots L$. As with the discrete angular distribution, these discrete energy-losses and weights give $2L$ free parameters with which we can preserve exactly $2L$ energy-loss moments. The advantage of this approximate cross section is that we now have a systematic method of preserving energy-loss moments to a desired order. For every discrete energy-loss we add to the distribution, we preserve two additional energy-loss moments.

Preserving the moments requires that we set the energy-loss moments of Eq.(5) to the exact energy-loss moments. For example, if we use $L = 1$ so that we preserve the first two energy loss moments, we form the following non-linear system of algebraic equations,

$$\begin{aligned} Q_1 &= \alpha_1 \overline{Q}_1, \\ Q_2 &= \alpha_1 \overline{Q}_1^2, \end{aligned} \tag{6}$$

where Q_1 and Q_2 are the exact moments of the Møller differential energy-loss cross section. Using substitution, the system can be solved for α_1 and $\overline{Q}_1$ in terms of Q_1 and Q_2,

$$\overline{Q}_1 = \frac{Q_2}{Q_1}, \tag{7}$$

$$\alpha_1 = \frac{Q_1^2}{Q_2}. \tag{8}$$

Because we set the first and second moments of Eq.(5) to the exact moments of the appropriate energy-loss distribution, we are exactly preserving the first two energy-loss moments of the total cross section. However, by only preserving these two low order moments, we are essentially approximating the total cross section and all higher order moments by Q_1 and Q_2.

2.1.2 Higher Order Approximations

For higher order approximations (i.e., $L > 1$), there is no simple analytic solution for the non-linear system of equations. It is possible that one could solve the system using a Newton iteration scheme, but convergence is observed to be very slow. Sloan [11] reworked an algorithm in the code MORSE [10] to calculate discrete angles and corresponding weights using a Radau quadrature. The original MORSE implementation used a gauss quadrature to produce angles and weights, preserving the Legendre moments of the angular scattering distribution. The refined method uses the Legendre coefficients, given by the Legendre moments of the elastic cross section,

$$\Sigma_{l,el,leg}(E) = 2\pi \int_{-1}^{1} \mathrm{d}\mu_0 P_l(\mu_0)\Sigma_{el}(E,\mu_0),\ l = 1, 2\ldots, \tag{9}$$

where $P_l(\mu_0)$ are the Legendre polynomials of μ_0. The Legendre coefficients are given by,

$$f_l = \frac{\Sigma_{l+1,el,leg}}{\Sigma_{0,el,leg}},\ l = 0, 1, 2\ldots. \tag{10}$$

Sloan's revision to the MORSE algorithm uses the calculated Legendre coefficients and first calculates Gauss moments, and using differences between successive Gauss moments, Radau moments are generated. The algorithm preserves the total cross section and $2L$ moments in $L + 1$ angles, where the forward angle, $\mu_0 = 1$, is always preserved. Using the Radau quadrature solution, the distribution can now be represented as

$$\Sigma^*_{el}(E,\mu_0) = \frac{\gamma_0}{2\pi}\delta[\mu_0 - 1] + \sum_{l=1}^{L} \frac{\gamma_l(E)}{2\pi}\delta[\mu_0 - \xi_l(E)],\ l = 1, 2\ldots, \tag{11}$$

where the forward direction $\mu_0 = 1$ represents a collision in which no scattering occurs at all. Knowing this we can essentially eliminate the delta function for the forward direction from Eq.(11), to get

$$\Sigma^*_{el}(E,\mu_0) = \sum_{l=1}^{L} \frac{\gamma_l(E)}{2\pi}\delta[\mu_0 - \xi_l(E)], \tag{12}$$

and we can now calculate the corresponding total cross section as

$$\Sigma^*_{el}(E) = \left(\sum_{l=1}^{L} \gamma_l\right) - \gamma_0, \tag{13}$$

where $\Sigma^*_{el}(E)$ is now reduced by the weight of the forward direction, and thus gives a reduction in the total cross section and an increase in the mean free path. In other words, the use of the forward angle has preserved the higher order moments of the distribution, and yielded a system with a cross section that is smaller in magnitude and less forward peaked than the analog cross section.

2.1.3 Linear Mapping from Energy to Angle

The underlying similarities between elastic and inelastic scattering cross sections lead to using the algorithm developed by Sloan as a method to solve for $\overline{Q}_l$ and α_l from Eq.(5). As mentioned previously, this algorithm uses the Legendre coefficients of the elastic scattering differential cross section.

Given an energy-loss cross section (i.e., the Møller), we wish to map the cross section $\Sigma_{e^-}(E,Q)$, $0 < Q < Q_{max}$, to a pseudo-scattering cross section $\widetilde{\Sigma}(E,\mu_0)$, for $-1 < \mu_0 < 1$. Here, μ_0 is the directional cosine of the pseudo-scattering angle, and we constrain $\widetilde{\Sigma}(E,\mu_0)$ so that the momentum transfer moments, $\Sigma_{l,el,mom}$, or the Legendre moments, $\Sigma_{l,el,leg}$ can be related directly to the energy-loss moments (Eq.(2)). This constraint is achieved by assuming a one-to-one relationship between μ_0 and Q, so that we have

$$2\pi\widetilde{\Sigma}(E,\mu_0)\mathrm{d}\mu_0 = \Sigma_{e^-}(E,Q)\mathrm{d}Q. \tag{14}$$

If we further assume that we have a known invertible mapping, i.e.,

$$Q = T(\mu_0), \tag{15}$$
$$\mu_0 = T^{-1}(Q), \tag{16}$$

we can obtain an explicit pseudo-scattering cross section from using the energy-loss cross section, given by

$$\widetilde{\Sigma}(E,\mu_0) = \frac{1}{2\pi}\Sigma[T(\mu_0)]\left|\frac{\mathrm{d}T}{\mathrm{d}\mu_0}\right|. \tag{17}$$

Because we have assumed a one-to-one relationship, we can form the linear mapping of the form

$$Q = T(\mu_0) = a + b\mu_0, \tag{18}$$

where a and b are selected such that $T(1) = 0$ and $T(-1) = Q_{max}$, i.e., a forward scatter corresponds to zero energy-loss and a backscatter corresponds with a maximum energy-loss. Using these conditions, we find the following mapping:

$$Q = T(\mu_0) = \frac{Q_{max}}{2}(1-\mu_0), \tag{19}$$

and its inverse

$$\mu_0 = T^{-1}(Q) = 1 - \frac{2Q}{Q_{max}}. \tag{20}$$

In the case that the cross section for $Q < Q_{min}$ is not defined, we set $\Sigma(E,Q) = 0$ for $0 \le Q < Q_{min}$, giving us a cutoff value for μ_0 of

$$\mu_{cut} = 1 - \frac{2Q_{min}}{Q_{max}}, \tag{21}$$

in turn giving an analogous condition on the pseudo-scattering cross of $\widetilde{\Sigma}(E,\mu_0) = 0$ for $-1 \le \mu_0 < \mu_{cut}$.

With these relationships, we can now directly calculate either the Legendre or momentum-transfer moments of the pseudo-scattering cross section directly, and obtain the Legendre coefficients necessary for refined MORSE algorithm to create pseudo-scattering angles and their corresponding weights.

We also present an alternative method for finding the Legendre coefficients using a direct relationship between the energy-loss moments of the inelastic scattering cross section and the momentum transfer moments of the pseudo-scattering cross section (using the linear mapping from energy to angle). With the momentum transfer moments of the pseudo-scattering cross section, we can form a direct relationship between the momentum transfer moments and the energy loss moments. Manipulating Eq.(19) we obtain the following relationship between Q and $(1-\mu_0)$

$$1-\mu_0 = \frac{2Q}{Q_{max}}. \tag{22}$$

Using Eq.(22) in Eq.(4), we can now represent the momentum transfer moments directly in terms of the energy-loss moments:

$$\widetilde{\Sigma}_{l,el,mom} = \left(\frac{2}{Q_{max}}\right)^l \int_{Q_{min}}^{Q_{max}} Q^l \Sigma_{e^-}(E,Q), \tag{23}$$

where we can see that the integral in Eq.(23) is exactly equivalent to Eq.(2). The direct relationship between the energy-loss moments and the momentum transfer moments is then given by

$$\widetilde{\Sigma}_{l,el,mom}(E) = \left(\frac{2}{Q_{max}}\right)^l Q_l, \tag{24}$$

where Q_l are the energy-loss moments. To obtain the Legendre coefficients, however, we must now relate the momentum transfer moments to the Legendre moments. To do this, we first perform a Taylor series expansion of $P(\mu_0)$ about $(1-\mu_0)$, which is shown as

$$P_l(\mu_0) = P_l(1-(1-\mu_0)) = \sum_{n=0}^{l} c_n \frac{(-1)^n}{n!}(1-\mu_0)^n, \tag{25}$$

where c_n are dependent on the Legendre polynomials [12], and given as

$$c_n^l = \frac{\mathrm{d}^n}{\mathrm{d}{\mu_0}^n} P_l(\mu_0)\Big|_{\mu_0=1}. \tag{26}$$

The Taylor series expansion in Eq.(25) truncates at $n=l$ due to the fact that P_l is a polynomial of degree l and only has a maximum of l nonzero derivatives. The recursion relationship for c_n^l [13] is given by

$$c_n^l = \frac{1}{2^n n!} \prod_{i=0}^{n-1} [l(l+1) - i(i+1)]. \tag{27}$$

Using the pseudo-scattering cross section and Eq.(25) in Eq.(9), we obtain

$$\widetilde{\Sigma}_{l,el,leg}(E) = \sum_{n=0}^{l} c_n^l 2\pi \int_{-1}^{1} \mathrm{d}\mu_0 (1-\mu_0)^n \widetilde{\Sigma}(E,\mu_0), \tag{28}$$

where the integral on the right hand side of the equation is equivalent to the momentum transfer moments given by Eq.(4), so we can now represent the Legendre moments of the pseudo-scattering cross section in terms of the momentum transfer cross section:

$$\widetilde{\Sigma}_{l,el,leg}(E) = \sum_{n=0}^{l} c_n^l \widetilde{\Sigma}_{n,el,mom}(E). \tag{29}$$

With Eq.(24), we now can represent the Legendre moments in terms of the exact energy-loss moments (Q_n) of the appropriate differential energy-loss cross section as

$$\widetilde{\Sigma}_{l,el,leg}(E) = \sum_{n=0}^{l} c_n^l \left(\frac{2}{Q_{max}}\right)^n Q_n. \tag{30}$$

We can further simplify $\widetilde{\Sigma}_{l,el,leg}(E)$, due to the fact that for all n at $l = 0$ we have $c_n^0 = 1$, and for all $n = 0$ for $l = 1, 2 \ldots$, $c_0^l = 0$, we can write Eq.(30) in terms of the reduced total cross section, given by

$$\widetilde{\Sigma}_{l,el,leg}(E) = Q_0 + \sum_{n=1}^{l} c_n^l \left(\frac{2}{Q_{max}}\right)^n Q_n \tag{31}$$

Using the refined scattering algorithm from MORSE, the discrete scattering angles and their corresponding weights can now be calculated. From these discrete angles we can use the prescribed mapping (i.e., Eq.(18)) to map from the pseudo-scattering angle back to energy to obtain our discrete energies, $\overline{Q}_l$. These discrete energies will be comprised of $\overline{Q}_0 = Q_{min}$, and $\overline{Q}_l$ for $l = 1, 2 \ldots L$, preserving $2L$ moments of the energy-loss cross section. The weights, γ_l, are obtained from the original relationship for $\widetilde{\Sigma}(E, \mu_0)$ in Eq.(17). Using our discrete cross sections for energy-loss (Eq.(5)) and angle (Eq.(3)) in Eq.(17), we find that $\alpha_l = \gamma_l$, for all l.

It is important to note that with Eq.(30), it is no longer necessary to have an explicit differential energy-loss cross section. Although this feature of the linear mapping is not discussed in this paper, if the energy-loss moments are known (either experimentally or empirically derived energy-loss moments) it would be possible to calculate the Legendre coefficients necessary to generate a discrete energy-loss distribution.

2.1.4 Hybrid Discrete-Continuous Energy-Loss Model

The motivating factor with this model completely lies with the fact that high energy-loss collisions only occur a small fraction of time compared to low energy-loss collisions. If we represent the low energy-loss collisions by a discrete distribution and represent the large energy-losses exactly, it is possible to smooth artifacts caused by the discrete distribution. Discrete collisions can be smoothed if there are large numbers of collisions that occur before the quantity of interest is calculated (i.e., energy-loss spectra or dose). With energy-loss spectra, especially for thin slabs, there are large numbers of small energy-loss collisions, but for the larger energy-loss collisions there are not enough collisions that could smooth a purely discrete distribution. If we represent only the small energy-losses by the discrete energy-loss distribution, it is possible that the large number of collisions of these small energy-loss will smooth out the discrete distribution in this portion of energy-loss spectra. In addition, representing the larger energy losses by the analog cross section will of course yield exact results for higher energy transfers.

The decomposition of the distribution, so that we use a discrete cross section to represent the low energy losses by a discrete distribution and the high energy losses by the continuous analog distribution, is performed by creating a cutoff or interpolating parameter, Q^*. With Q^* we now have our hybrid cross section, given by

$$\Sigma_{e^-}(E, Q)\mathrm{d}Q = \begin{cases} \Sigma^*_{e^-}(E, Q)\mathrm{d}Q & , \quad Q_{min} \leq Q \leq Q^* \\ \Sigma_{e^-}(E, Q)\mathrm{d}Q & , \quad Q^* < Q \leq Q_{max} \end{cases} \tag{32}$$

It is highly desirable that the Q^* is chosen so that it not only represents enough of the low energy-losses so that the total mean free path from the hybrid total cross section will be reduced significantly, but still retain enough of the high energy-loss portion of the cross section so that there are no discrete artifacts due to the discrete distribution. Here we propose a method of determining Q^*, such that the mean free path of the distribution for $Q^* \leq Q \leq Q_{max}$ can be preset. This gives us the following equation from which we can solve for Q^*,

$$\frac{1}{\lambda} = \int_{Q^*}^{Q_{max}} \Sigma_{e^-}(E, Q)\mathrm{d}Q, \tag{33}$$

where λ is the mean free path of the high energy-loss portion of the distribution which can be represented in terms of the total energy-loss cross section,

$$\Sigma_{e^-}(E) = \frac{1}{\lambda}. \tag{34}$$

We are free to choose the mean free path in Eq.(33)to optimize efficiency and accuracy. This is a very attractive feature of our hybrid method, as the mean free path of our distribution for $Q > Q^*$ will determine how much of the distribution will be represented by the discrete distribution. The choice of mfp for $Q > Q^*$ is constrained by the need to ensure that a sufficient number of large energy-loss collisions occur while at the same time making sure that the associated cross section is small enough that we significantly reduce the total cross section of the entire distribution. It is also important to note that because we have the freedom of choosing the mean free path of the continuous portion of the cross section, as Q^* approaches Q_{min}, the total mean free path of the entire distribution approaches the analog mean free path. Thus we have the potential of achieving an arbitrary degree of accuracy.

To provide a systematic method in which we can calculate Q^*, we preserve the mean free path for $Q > Q*$ as one condensed history "step size". Preserving the mean free path as a step size now gives us the following relationship for Q^*,

$$\frac{1}{\lambda_{CH}} = \int_{Q^*}^{Q_{max}} \Sigma_{e^-}(E, Q)\mathrm{d}Q, \tag{35}$$

where λ_{CH} is the condensed history step size. Using the Møller differential cross section we can now calculate Q^*.

2.2. Implementation in MCNP

We have implemented our new straggling model in MCNP using the following algorithm that avoids the need for a precomputed spectrum. The electron is transported through the step using a single event Monte Carlo simulation based on the moment-preserving model cross sections described above, and the exiting energy is taken to be the incident energy for the next step. This is done for each history for successive steps until the electron is terminated. Since our approach solves the exact transport equation (without deflection), the exiting energy represents a valid sample from the exact energy distribution at the end of the step. That is, the statistically converged (with respect to the number of electron histories) straggling distribution obtained using this method constitutes a solution of Eq.(1) with the approximate cross section. Although not as fast as sampling a precomputed distribution, the use of smooth cross sections with associated mean free paths that are long compared to analog but sufficiently short compared to a step size, ensures that the Monte Carlo solution does not incur an excessive additional computational cost.

In our modification of MCNP, an option in the MCNP input deck allows for the use of either the Landau straggling model or the above moment-preserving model thereby facilitating a direct comparison of the two

approaches. We note that for these comparisons to be meaningful it is necessary to ensure that the sole free parameter in the Landau distribution, namely the mean energy loss, or stopping power, is identical to that used in the new model. In generating numerical results, we have used the stopping power from the Møller cross section in both implementations. We have also implemented a third option, namely the solution of the analog problem using the same single event Monte Carlo logic as for the modeled cross section. This provides a means of benchmarking the two approximate straggling methods as well as a measure of computational efficiency realized with these methods. Finally, we mention that the angular deflections are described using the existing Goudsmidt-Saunderson multiple scattering model in MCNP for each of the three energy straggling options described above, although we point out here that our eventual goal is to implement a strategy for obtaining the electron direction at the end of a step which is similar to that described above for straggling.

3. Numerical Results and Discussion

In this section we present illustrative numerical results for energy spectra and dose distributions, comparing predications from the existing straggling model in MCNP and our new approach against analog results.

Figure 1 displays the transmitted energy spectra for a 10 MeV electron beam incident on a 0.68 cm slab of water, equivalent to a single step. While the purely discrete model shows the anticipated artifacts (heightened by virtue of the extremely thin target layer), the accuracy of the hybrid model, on the other hand, is outstanding. The Landau straggling distribution is accurate over the higher energy part of the spectrum but displays a prolonged tail, the well-known artifact resulting from the preset cut-off designed to make the mean energy loss finite.

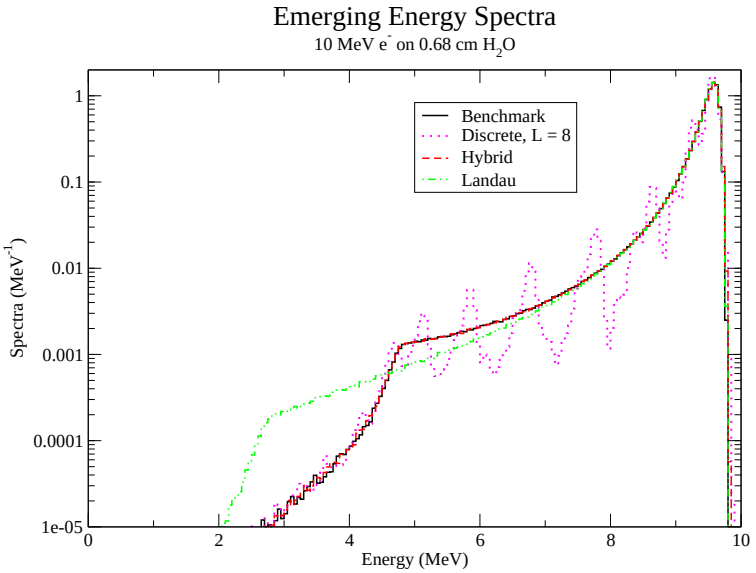

Figure 1. Emerging Energy Spectra for 10 MeV e^- incident on a 0.68 cm slab of H_2O

Table I shows radial and axial leakages, as well as cpu times, from a cylinder of radius 0.5 cm and height 1.5 cm for a 10 MeV beam of electrons incident on axis. The accuracy of all models is exceptional for the

radial and transmitted leakages, but particularly noteworthy is that a very low order purely discrete model suffices to also give very accurate results. While the same cannot be said for the backscattered or reflected current the results are nevertheless very satisfying. All problems were run on the same single processor (3GHz, Pentium 4) and MCNP was compiled using the Intel 8.0 compiler with no optimizations. From these runtimes, we see that all of the methods result in dramatic speedups over the benchmark solution and while the expense of our new method increases with increasing numbers of moments preserved, the penalty relative to sampling Landau is not excessive.

Table I. Surface Current Tallies and Runtimes, 10 **MeV on** H_2O **Cylinder (R=0.5 cm,Z=1.5 cm)**

Model	z=0.0 cm	z = 1.5 cm	r = 0.5 cm	Runtime
Benchmark	$5.7100\text{x}10^{-5}$	$9.1340\text{x}10^{-1}$	$8.6542\text{x}10^{-2}$	367.79
Landau	$5.9200\text{x}10^{-5}$	$9.1280\text{x}10^{-1}$	$8.7135\text{x}10^{-2}$	8.24
Disc. L=1	$5.4900\text{x}10^{-5}$	$9.1249\text{x}10^{-1}$	$8.7456\text{x}10^{-2}$	7.18
Disc. L=4	$5.5600\text{x}10^{-5}$	$9.1357\text{x}10^{-1}$	$8.6369\text{x}10^{-2}$	8.26
Disc. L=8	$5.7200\text{x}10^{-5}$	$9.1335\text{x}10^{-1}$	$8.6591\text{x}10^{-2}$	12.99
Hybrid	$5.9300\text{x}10^{-5}$	$9.1351\text{x}10^{-1}$	$8.6426\text{x}10^{-2}$	16.61

In Figure 2 we show radial dose profiles at three different locations in a cylinder of water with a radius of 5 cm and a height of 10 cm, again for a 10 MeV electron pencil beam on axis. The dose profiles were computed at $z = 1$ cm and $z = 4$ cm, with axial thickness of 1 cm, and at $z = 8$ cm with thickness of 2 cm, and with radial cell width 0.1 cm at all locations. Once again, the accuracy of the hybrid model is uniformly outstanding, as is also the case for the standard model using Landau. The purely discrete model with four discrete energy-losses (preserving eight moments) also gives results that are barely distinguishable from the other models, while even a single discrete energy-loss model (preserving just two moments) is capable of yielding useful results.

Finally, in Figures 3, 4, and 5 we show the radial dose profiles for three different simulations, with cylinders of silicon located within a cylinder of water, similar to the above cylinder of water (i.e., a cylinder of radius 5 cm and a height of 10 cm). Also, similar to Figure 2, the radial dose profiles are of cylinders with radial cell widths of 0.1 cm and with axial thickness of 1 cm located at $z = 1$ cm and $z = 4$ cm (Figures 3 and 4), and a cylinder of axial thickness of 2 cm located at $z = 8$ cm (Figure 5). It should also be noted that these simulations were run with 10^8 electrons. Included in each figure is the benchmark for the simulation with Si in the cylinder and the appropriate approximations, and for comparison, the benchmark with H_2O in the cylinder. In Figure 3, we see the dose is primarily distributed in the center of the Si cylinder. The dose in this region is approximated with high accuracy for all of the approximate methods. It is also evident that for the purely discrete model, only four discrete energies are required to obtain an accurate approximation. Figure 4 is more interesting, as it demonstrates the effectiveness of the approximations as the electron beam spreads due to scattering. As with the previous Si cylinder, the hybrid and Landau simulations are highly accurate and indistinguishable from the benchmark. The purely discrete model, while preserving only two moments, provides even a fairly accurate approximation. Preserving 8 moments, using 4 discrete energies, provides a result that is indistinguishable from the benchmark as well.

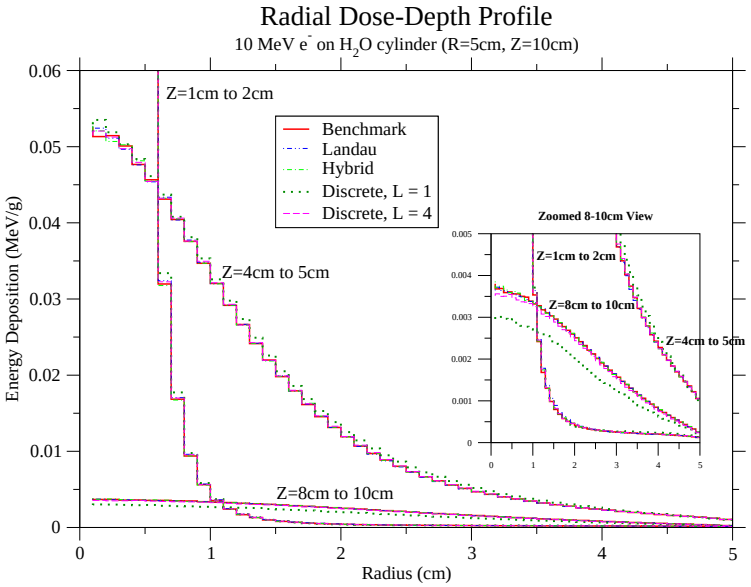

Figure 2. Radial Dose Profile for 10 MeV e^- on H_2O Cylinder (Radius of 5 cm and Height of 10 cm, at Depths from z=1 cm to 2 cm, z=4 cm to 5 cm and z=8 cm to 10 cm)

In Figure 5, we see that the beam has spread much more and much of the energy of the incident electrons has been absorbed earlier in the cylinder. Again, the Landau and the hybrid models provide excellent approximations to the benchmark. The purely discrete model, however, underestimates the dose deposited in the Si cylinder for both the $L = 1$ and $L = 4$ (which still gives a fairly accurate approximation) models. Due to the increasing accuracy obtained with increasing the number of preserved moments, by preserving 16 moments using 8 discrete energies, we are able to obtain a highly accurate solution.

4. CONCLUSIONS

We have demonstrated a new energy straggling model for use with the condensed history algorithm in MCNP. A modeled energy-loss cross section, which eliminates the singularity in the analog cross section at zero energy transfer while retaining important physical characteristics of the analog slowing down process, has been used in conjunction with a single event Monte Carlo simulation through every CH step to show that highly accurate energy spectra and dose profiles can be obtained. Our method is potentially more accurate than the standard Landau straggling model with only a small increase in computational cost.

REFERENCES

[1] M.J. Berger, “Monte Carlo Calculations of the Penetration and Diffusion of Fast Charged Particles,” in *Methods in Computational Physics*, Vol. 1, & edited by B. Adler, S. Fernbach and M. Rotenberg, Academic Press, New York (1963).

[2] S.M. Seltzer, “Electron-photon Monte Carlo Calculations: The ETRAN Code,” *Appl. Radiat. Isot.*, **vol. 42, no. 10**, pp. 917-941 (1991).

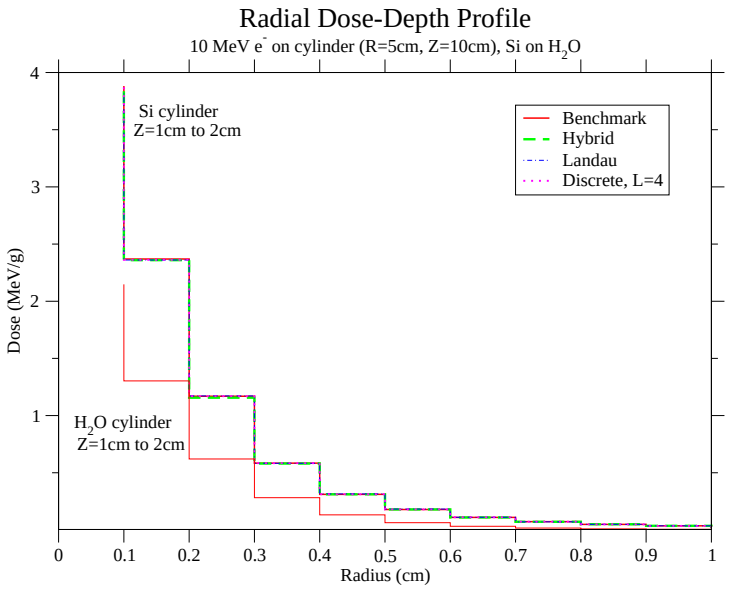

Figure 3. Radial Dose Profile for Si Cylinder of axial thickness 1 cm at $z = 1\ cm$ in H_2O Cylinder (Radius of 5 cm and Height of 10/unitscm), 10 $MeV\ e^-$ incident at $z = 0\ cm$.

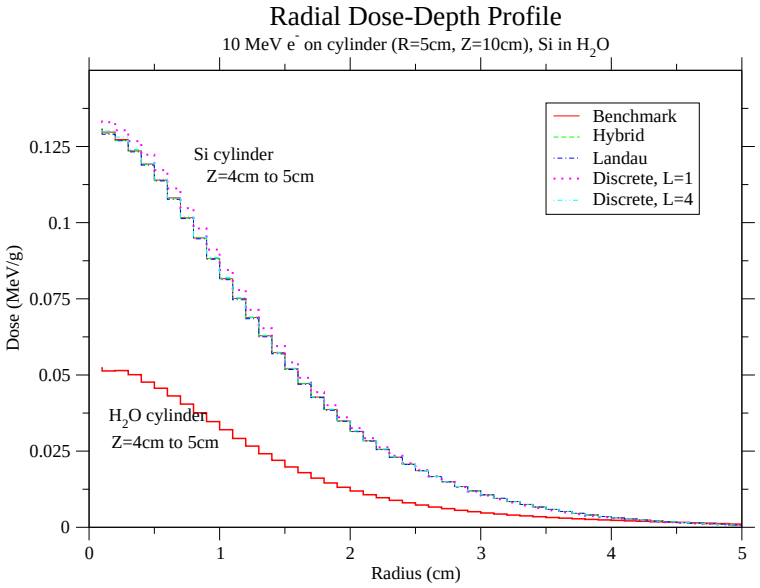

Figure 4. Radial Dose Profile for Si Cylinder of axial thickness 1 cm at $z = 4\ cm$ in H_2O Cylinder (Radius of 5 cm and Height of 10/unitscm), 10 $MeV\ e^-$ incident at $z = 0\ cm$.

[3] X-5 MCNP Development Team, "MCNP - A General Purpose Monte Carlo N-Particle Transport Code, Version 5," *Technical Report LA-UR-03-1987*, LANL, (2003).

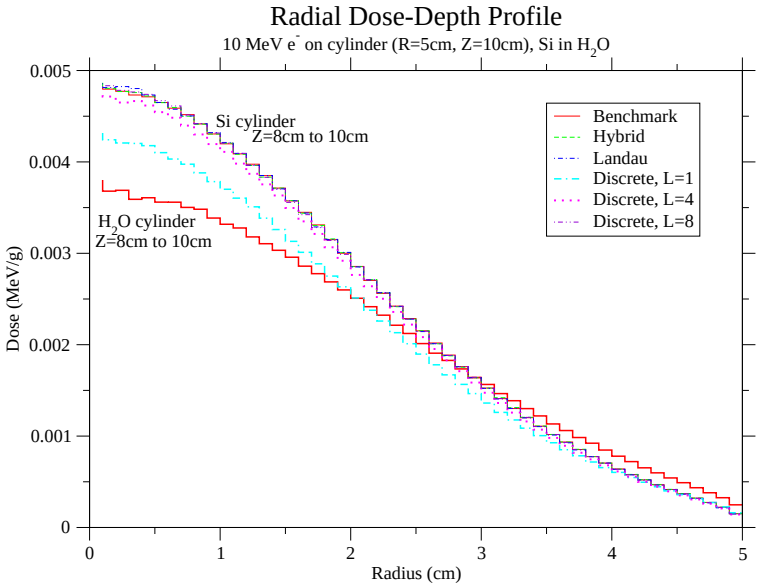

Figure 5. Radial Dose Profile for Si Cylinder of axial thickness 2 cm at $z = 8\ cm$ in H_2O Cylinder (Radius of 5 cm and Height of 10/unitscm), 10 $MeV\ e^-$ incident at $z = 0\ cm$.

[4] J.A. Halbleib, R.P. Kensek, T.A. Mehlhorn, G.D. Valdez, S.M. Seltzer and M.J. Berger, "ITS version 3.0: The Integrated TIGER Series of Coupled Electron/Photon Monte Carlo," *Technical Report SAND91-1634*, SNL (1992).

[5] B. Franke and A.K. Prinja, "Monte Carlo Electron Dose Calculations using discrete angles and Discrete Energy Losses," *Nuclear Science and Engineering*, **vol. 149**, pp. 1-22 (2005).

[6] H.G. Hughes and R.E. Prael, "Modeling Charged-Particle Energy-Loss Straggling," *Technical Report LA-UR-03-3898*, LANL (2003).

[7] L.T. Harding and A.K. Prinja, "Energy-Loss Straggling for Electrons and Positrons Using Moment Preserving Methods," *Trans. Am. Nucl. Soc.*, Washington, D.C., Nov., 2005, Vol. 93, p. 453 (2005).

[8] R.D. Evans, *The Atomic Nucleus*, McGraw-Hill, New York (1976).

[9] L.T. Harding, *Monte Carlo Simulations of Electron and Positron Energy-Loss Straggling*, Master's Thesis, University of New Mexico (2005).

[10] E.A. Straker et. al., "MORSE Code - A Multigroup Neutron and Gamma-Ray Monte Carlo Transport Code," *Technical Report ORNL-4716*, ORNL (1970).

[11] D.P. Sloan, "A New Multigroup Monte Carlo Scattering Algorithm Suitable for Neutral and Charged-Particle Boltzmann and Fokker-Plank Calculations," *PhD Thesis*, University of New Mexico (1983).

[12] G.C. Pomraning, "Higher Order Fokker-Planck Operators," *Nuclear Science and Engineering*, **vol. 124**, p. 390, 1996.

[13] A.K. Prinja and G.C. Pomraning, "A Generalized Fokker-Planck Model for Transport of Collimated Beams," *Nuclear Science and Engineering*, **vol. 137**, p. 227, 2001.